Chemical Physics Letters 467 (2009) 339–343

Contents lists available at ScienceDirect

Chemical Physics Letters

journal homepage: www.elsevier.com/locate/cplett

The ^{13}C NMR properties of low hydroxylated fullerenes with density functional theory

Eudes E. Fileti [a], Roberto Rivelino [b,*]

[a] CCNH, Universidade Federal do ABC, 09210-270, Santo André, SP, Brazil
[b] Instituto de Física, Universidade Federal da Bahia, 40210-340, Salvador, BA, Brazil

ARTICLE INFO

Article history:
Received 20 September 2008
In final form 10 November 2008
Available online 14 November 2008

ABSTRACT

Work presented here applies density functional theory to investigate the chemical shifts and hyperfine coupling constants in fullerenols. The magnetic effects of adding one hydroxyl group on the carbon cage of C_{60} are carefully examined on this base. Calculations make evident that unpaired spins are highly localized on the fullerene surface. Also, the addition of three hydroxyl groups on C_{60} reveals a pattern of spin density distribution very similar to that obtained for $C_{60}OH$, which can indicate a high radical reactivity of fullerenols containing an odd number of hydroxyl groups and, thus, a tendency to form polyhydroxylated systems.

Nuclear magnetic resonance (NMR) spectroscopy has been utilized with great success to characterize diverse fullerene-based materials [1–8]. Among their applications, NMR parameters are related to the structural features of single molecules and can provide useful information to identify chemical changes. Recently, endohedral magnetic shielding of fullerenes has experimentally been investigated [7] and calculations have been carried out using density functional theory (DFT) [8]. As other important application, ^{13}C NMR spectroscopy has been employed to investigate the reactivity of water-soluble C_{60} with ozone dissolved in aqueous solutions [9], revealing a high level of functionalization and considerable loss of I_h symmetry of C_{60}. Because of the high radical reactivity of fullerenes [10], they can be easily transformed into polyfunctionalized fullerene-derivatives [11]. Considering the water-soluble fullerene-based systems, $C_{60}(OH)_n$ (fullerenols) are relatively easy to be synthesized [12] and have been proposed as promising biocompatible materials [13]. On the other hand, although some experimental studies are reporting on the NMR properties in connection with the reactivity of fullerenols [9,12], little information is available on the changes of the ^{13}C NMR parameters after hydroxylation.

In this Letter, we examine the theoretical ^{13}C NMR chemical shifts of $C_{60}(OH)_{1-3}$ isomers, taking into account the hyperfine coupling constants in $C_{60}OH$ and $C_{60}(OH)_3$ doublet states by using DFT [14]. Recent theoretical developments for paramagnetic systems are given in Refs. [15,16]. Here, these compounds are taken as model systems to understand the polyhydroxylation mechanism of fullerenes that usually occurs in the presence of radical species [9–12]. In our computational strategy, (i) we fully optimize the geometries and calculate the electronic structure of the fullerenols within the B3LYP hybrid scheme [17] with the 6-31G(d,p) Gaussian basis set; and (ii) we calculate the NMR properties within the gauge-independent atomic orbital (GIAO) approach [18] at the B3LYP/6-31G(d,p) level. Items (i) and (ii) are carried out as implemented in the GAUSSIAN 03 program [19]. This methodology has produced an excellent performance on the ^{13}C NMR chemical shifts of diverse fullerene-related systems [4,8]. The inclusion of the exact (Hartree–Fock) exchange with local and gradient-corrected exchange and correlation terms seems to be relevant, so that B3LYP performs much better than pure GGA functionals which tend to underestimate the NMR chemical shifts [20].

Within the above methodology, we have calculated the isotropic ^{13}C NMR shielding and its anisotropy (σ_{iso} and σ_{anis}, respectively [21]) of the carbon atoms of the fullerenols and C_{60} (to be used as a reference). Thus, we obtain the usual isotropic chemical shift (δ_{iso}) [22–24]

$$\delta_{iso} = \sigma_{iso}(C_{60}(OH)_n) - \sigma_{iso}(C_{60}). \quad (1)$$

For the anisotropy shielding, we obtain the anisotropic chemical shift as given by

$$\delta_{anis} = \sigma_{anis}(C_{60}(OH)_n) - \sigma_{anis}(C_{60}). \quad (2)$$

We note that Eq. (2) is different from the chemical shift anisotropy (CSA) mechanism, however it is commonly used to describe the CSA autocorrelation properties [24].

In NMR spectroscopy, a standard system is chosen as a reference, thus the chemical shift is taken as the shielding difference between the atom of interest and the corresponding atom in the reference system. In the theoretical calculations, the magnetic shielding must then be subtracted from the shielding in the

* Corresponding author. Fax: +55 71 3283 6606.
E-mail addresses: fileti@ufabc.edu.br (E.E. Fileti), rivelino@ufba.br (R. Rivelino).

0009-2614/$ - see front matter © 2008 Elsevier B.V. All rights reserved.
doi:10.1016/j.cplett.2008.11.035

Table 1
Isotropic, δ_{iso}, and anisotropic, δ_{anis}, ^{13}C NMR chemical shifts of $C_{60}OH$ calculated at the B3LYP/6-31G(d,p) level.

Upfield (more shielded in ppm)				Downfield (more deshielded in ppm)			
Atom	δ_{iso}	Atom	δ_{anis}	Atom	δ_{iso}	Atom	δ_{anis}
C1	59.59	C16	11.36	C3	−11.51	C1	−131.39
C6	3.84	C15	11.21	C4	−11.45	C2	−47.12
C9	3.79	C18	7.13	C13	−5.02	C5	−22.46
C5	3.76	C17	6.89	C2	−5.01	C10	−22.43
C10	3.71	C20	6.80	C12	−4.06	C6	−14.44
		C19	6.72	C11	−4.04	C9	−14.25

The atoms sites are indicated in the Schlegel diagrams (Fig. 1a).

Table 2
Isotropic Fermi contact, A_{iso}, and Mulliken spin density, ρ_s, of $C_{60}(OH)$ calculated at the B3LYP/6-31G(d,p) level.

Atom	A_{iso} (MHZ)	ρ_s (10^{-2})
C2	68.61	46.76
C10	34.92	24.77
C5	34.92	24.77
C23	15.22	10.93
C24	15.22	10.93
C15	−29.52	−14.70
C16	−29.52	−14.70
C21	−14.76	−6.95
C22	−14.76	−6.95

The atoms sites are indicated in the Schlegel diagrams (Fig. 1a) and the sign distribution is given in Fig. 2a.

reference system. In the differences given by the Eqs. (1) and (2), the reference values cancel out and, therefore, the chemical shifts are referred simply as the difference between the shielding of the carbon atom in the fullerenol and the shielding of the carbon atom in C_{60}. In addition, for the doublet systems, i.e., $C_{60}OH$ and $C_{60}(OH)_3$, we compute the isotropic contribution of the hyperfine coupling constants through the Fermi contact terms [14].

Our calculated chemical shielding for the carbon atoms in C_{60} is 50.50 ppm. This reference value will be used to calculate the chemical shifts of the fullerenols. As reported by Sun and Kertesz [4] the error in the theoretical chemical shielding is systematic for fullerenes and is significantly reduced when chemical shifts are used [5].

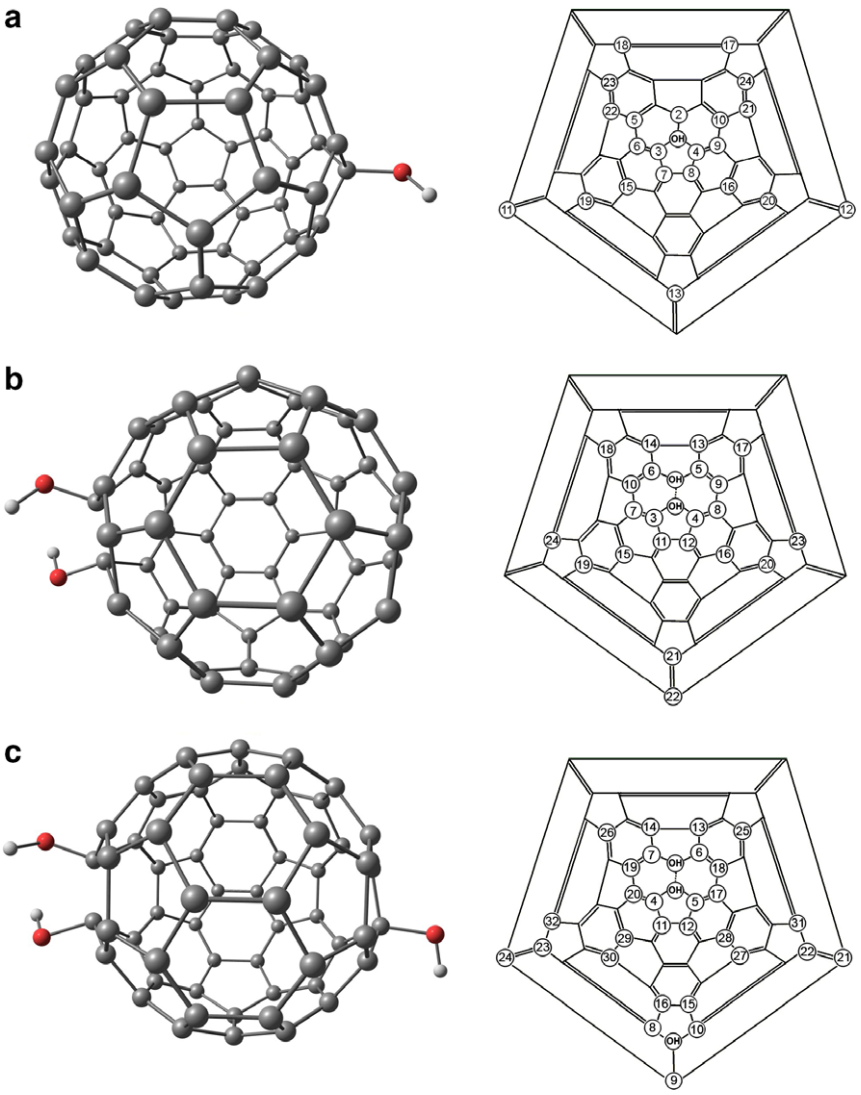

Fig. 1. Optimized structures of the fullerenols using B3LYP/6-31G(d,p) and their respective Schlegel diagram indicating the carbon sites with relevant calculated ^{13}C NMR properties. The labels of the hydroxylated carbon sites are not shown for clarity. In $C_{60}OH$ C1 is connected to C2, C3 and C4; in $C_{60}(OH)_2$ C1 is connected to C2, C3 and C4, while C2 is additionally connected to C5 and C6; and in $C_{60}(OH)_3$ C1 is connected to C8, C9 and C10, while C2 is connected to C3, C4 and C5, and C3 is additionally connected to C6 and C7.

Also, early DFT results have shown that the accuracy of the calculated chemical shifts compared to the experimental values is around 1 ppm [6]. Thus, some predicted chemical shifts and Fermi contact terms are presented in Tables 1–5.

As can be seen in Table 1, for $C_{60}OH$ the more shielded atoms, i.e., those with largest isotropic upfield chemical shifts (δ_{iso}), present small values for the anisotropic downfield chemical shifts (δ_{anis}). In this sense, the calculated δ_{iso} for the hydroxylated carbon site (C1 atom) gives 59.59 ppm with δ_{anis} of −131.39 ppm. Interestingly, the other shifted upfield sites are in *meta* and *para* positions with respect to the OH-adsorbed site, going clockwise in the left hexagon ring or counter-clockwise in the right hexagon ring (Fig. 1a). For example, C6 and C9 (*meta*-positioned) give δ_{iso} of 3.8 ppm and δ_{anis} of approximately −14 ppm, whereas C5 and C10 (*para*-positioned) give, approximately, δ_{iso} of 3.7 ppm and δ_{anis} of −22 ppm. On the other hand, the neighbors connected to C1 (C3 and C4 atoms indicated in Fig. 1a) are shifted downfield, as a result of the decreased strain in this region [25], with values of around −11.5 ppm for δ_{iso} and −8.5 ppm for δ_{anis}. These sites are, however, more deshielded compared to the C2 one, for which δ_{iso} is of −5 ppm; although δ_{anis} is of −47 ppm. As we have investigated before [26], the open-shell $C_{60}OH$ molecule exhibits a dangling bond at the first neighbor carbon site belongs to a pentagon ring vertex of the fullerene cage, which increases the electron density in this atom. Similarly, isotropic downfield shifts are calculated for the second neighbors C7 and C8 ($\delta_{iso} \approx -4$ ppm). It is also valuable to mention that the distant sites from C1–OH, i.e., C11 and C12 give $\delta_{iso} \approx -4$ ppm. However, the most similar isotropic shift to C2 site is calculated at C13, giving −5 ppm. From these analyses, the largest anisotropic upfield shifts are observed at sites from cap to equator. For instance, these are the cases of C15 and C16, with δ_{anis} over 11 ppm, and C17–C20 with δ_{anis} over 7 ppm, as given in Table 1.

To investigate the effect of net electronic spin, we analyze the isotropic Fermi contact term (A_{iso}) contribution and the Mulliken spin density (ρ_s) at some carbon sites of the doublet state $C_{60}OH$. As is well known, A_{iso} of a given nucleus is related to the interaction between the nuclear spin and the spin of the unpaired electron. This is of special importance in determining many observable effects in paramagnetic NMR spectroscopy [15,16,27]. The more sizeable values are presented in Table 2 and the coupling constants in all sites are represented in Fig. 2a. To visualize this effect within the one-particle framework, a plot of spin density is depicted in Fig. 3a. As discussed early, the electron density at the C2 atom increases significantly, compared to C3 and C4, leading to a less deshielded site. Considering the isotropic contribution of the hyperfine coupling constants, we obtain the highest value of the

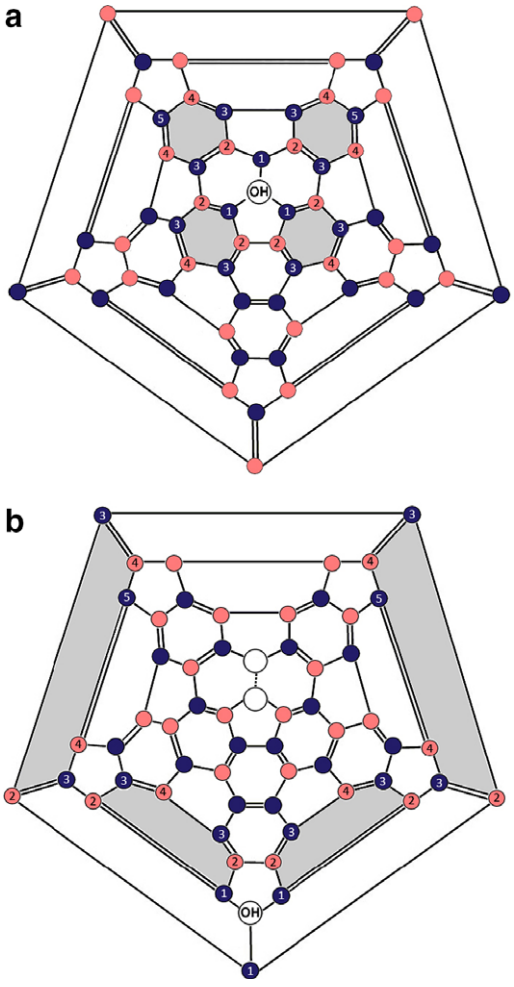

Fig. 2. Schlegel diagrams of (a) $C_{60}OH$ and (b) $C_{60}(OH)_3$ showing the calculated Fermi contact terms distribution: blue circles indicate positive values and red circles indicate negative values. Grey shading represents the adjacent hexagons, i.e., those connected to C1 or C2 in $C_{60}OH$ and connected to C1 or C9 in $C_{60}(OH)_3$. The order of the neighborhood is indicated by Arabic numbers. (For interpretation of the references to color in this figure legend, the reader is referred to the web version of this article.)

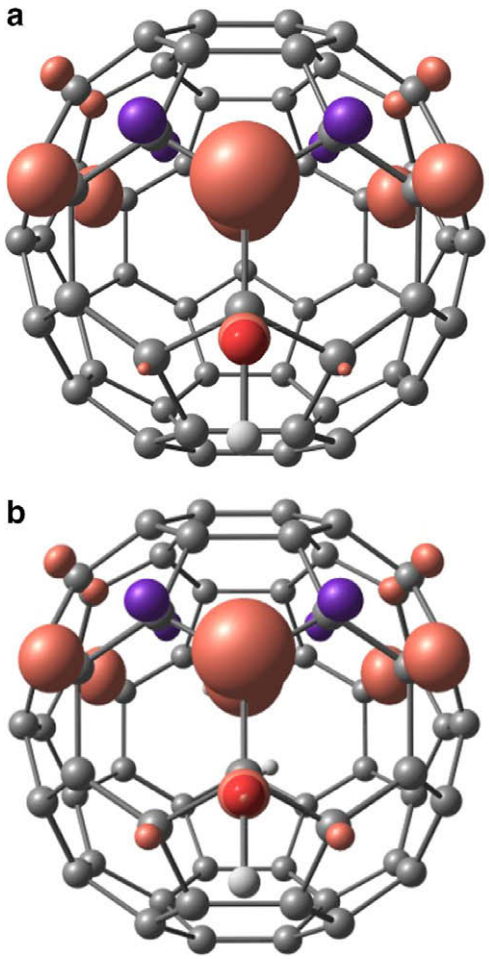

Fig. 3. Calculated spin densities of (a) $C_{60}OH$ and (b) $C_{60}(OH)_3$: red region indicates positive values and violet region indicates negative values. The isosurfaces in both cases are plotted with 0.01 au. (For interpretation of the references to color in this figure legend, the reader is referred to the web version of this article.)

Table 3
Isotropic, δ_{iso}, and anisotropic, δ_{anis}, ^{13}C NMR chemical shifts of $C_{60}(OH)_2$ calculated at the B3LYP/6-31G(d,p) level.

Upfield (more shielded in ppm)				Downfield (more deshielded in ppm)			
Atom	δ_{iso}	Atom	δ_{anis}	Atom	δ_{iso}	Atom	δ_{anis}
C2	51.12	C16	13.64	C5	−10.64	C2	−145.83
C1	51.05	C18	13.61	C3	−10.55	C1	−145.64
C10	6.36	C17	13.54	C6	−9.04	C10	−22.89
C8	6.24	C15	13.39	C4	−8.97	C7	−22.78
C9	6.21	C20	10.02	C22	−6.12	C9	−22.77
C7	6.21	C19	9.99	C21	−6.10	C8	−22.67

The atoms sites are indicated in the Schlegel diagrams (Fig. 1b).

Table 4
Isotropic, δ_{iso}, and anisotropic, δ_{anis}, ^{13}C NMR chemical shifts of $C_{60}(OH)_3$ calculated at the B3LYP/6-31G(d,p) level.

Upfield (more shielded in ppm)				Downfield (more deshielded in ppm)			
Atom	δ_{iso}	Atom	δ_{anis}	Atom	δ_{iso}	Atom	δ_{anis}
C3	58.76	C28	14.01	C8	−11.97	C1	−147.17
C1	51.20	C30	13.81	C10	−11.80	C2	−142.95
C2	50.16	C29	13.80	C4	−11.58	C3	−130.34
C19	5.93	C27	13.73	C5	−10.23	C9	−43.91
C18	5.93	C25	11.66	C7	−8.47	C19	−23.05
C17	5.51	C26	11.53	C6	−8.43	C18	−22.85
C20	5.93						

The atoms sites are indicated in the Schlegel diagrams (Fig. 1c).

Table 5
Isotropic fermi contact, A_{iso}, and Mulliken spin density, ρ_s, of $C_{60}(OH)_3$ calculated at the B3LYP/6-31G(d,p) level.

Atom	A_{iso} (MHZ)	ρ_s (10^{-2})
C9	71.63	48.39
C23	33.61	23.94
C22	33.45	23.83
C24	−29.61	−14.68
C21	−29.54	−14.63
C32	−14.22	−6.67
C31	−14.10	−6.60
C3	−20.11	−3.43

The atoms sites are indicated in the Schlegel diagrams (Fig. 1c) and the sign distribution is given in Fig. 2b.

calculated A_{iso} at C2 (68.61 MHz), with $\rho_s = 46.76 \times 10^{-2}$ that can be visualized in Fig. 3a. On the other hand, the other two first neighbors (i.e., C3 and C4) to the OH-adsorbed site, belonging to hexagon ring vertices, give A_{iso} of 13.81 MHz and ρ_s of 6.16×10^{-2}. Therefore whereas the highest NMR shielding is obtained at the C1 site, the highest Fermi contact coupling, along with the highest spin density, is obtained at the C2 site of $C_{60}OH$. This can be important to understand the adsorption process of a second hydroxyl group (containing one unpaired electron) at C2.

After the C2 site, the largest Fermi contact terms are obtained at C5 and C10 (34.92 MHz), exhibiting sizeable isotropic upfield chemical shifts, and at C23 and C24 (15.22 MHz), with negligible chemical shifts. Notice that these latter values are more similar to those calculated for the first neighbor sites C3 and C4 (13.8 MHz). Now, in contrast to C5 and C10 sites, C6 and C9 (also presenting upfield NMR chemical shifts of 3.8 ppm) give negative Fermi contact terms of −10.78 MHz. From these calculations, it is more interesting to realize the following Fermi contact distribution with respect to the OH-adsorbed site (see Fig. 2a): (1) positive values are obtained at all first neighbors; (2) negative values are obtained at all second neighbors; (3) positive values are again obtained at all third neighbors; (4) negative values are again obtained at forth neighbors, but only at site belonging to adjacent hexagon rings; (5) positive values are again obtained at fifth neighbors, but only at site belonging to adjacent hexagon rings; and (6) the rule is broken down for equatorial sites. In the opposite sense, considering C13 (A_{iso} = 5.38 MHz) as a new reference atom (see Fig. 1a), we obtain (7) negative values at first neighbors; (8) positive values at second neighbors; (9) negative values at third neighbors, and (10) positive values at forth neighbors, but at site belonging to adjacent hexagon rings. As we will analyze later, the addition of one OH group at C13 recovers rules (1)–(5) when both C1 and C2 are also hydroxylated sites.

Let us consider first the changes in the NMR chemical shifts due to the addition of a second hydroxyl group at the C2 site of $C_{60}OH$, forming the closed-shell $C_{60}(OH)_2$ fullerenol (Fig. 1b). Again, we observe that the hydroxylated atoms present the largest isotropic chemical shifts and smallest anisotropic shifts (see Table 3). As shown in Fig. 1b, the C1–OH site is connected to C2, C3 and C4; whereas C2–OH is connected to C6 and C5 (C1 and C2 are not represented for clarity). It is interesting, however, to notice here that the value of δ_{iso} at C1 (51.05 ppm) in $C_{60}(OH)_2$ is smaller than the corresponding value in $C_{60}OH$ (59.59 ppm) because of the hydroxylation at C2, presenting also a large isotropic chemical shift (51.12 ppm). Then, we note that the presence of a second hydroxyl group at C2 induces a mutual decrease of the chemical shift by approximately 8 ppm at C1 and C2. Also, as can be seen in Table 3, the calculated anisotropic chemical shifts give in this case more negative values of around −146 ppm. Here, the second neighbors to C1 (C7 and C8) and the third neighbors (C9 and C10), as displayed in Fig. 1b, give much larger isotropic upfield shifts (∼6 ppm) than the corresponding sites in $C_{60}OH$ (3.7–3.8 ppm). Additionally, in $C_{60}(OH)_2$ C7–C10 sites give δ_{anis} of −23 ppm, since all of them are second neighbors with respect to one hydroxyl group (at C1 or C2). Considering the largest anisotropic upfield shifts, we obtain at C15–C18 values in the range of 13.4–13.6 ppm (see Table 3), but with small isotropic downfield shifts around −3 ppm. Other interesting sites which we have taken into account here are C21 and C22, which are topologically equivalent to C13 in $C_{60}OH$ with respect to one OH group (see Fig. 1a and b), and shifted downfield with δ_{iso} of −6 ppm. Note that C21 and C22 are opposite sites to C1 and C2, respectively.

We explore now the effects of attaching other hydroxyl group at the C21 site of $C_{60}(OH)_2$, leading to the open-shell $C_{60}(OH)_3$ fullerenol. Some relevant calculated ^{13}C NMR shifts and Fermi contact terms are reported in Tables 4 and 5, respectively. Also, we discuss the spin density of $C_{60}(OH)_3$ in comparison with the $C_{60}OH$ system (Fig. 3a and b). As previously noted, the largest isotropic chemical shifts are obtained at hydroxylated sites, i.e., C1, C2 and C3 (Fig. 1c), which give, respectively, 50.16, 51.20 and 58.76 ppm. It is worth to observe here that the presence of a new OH group at C21 does not affect the chemical shifts calculated for C1–OH and C2–OH, once their values are rather similar to those obtained in $C_{60}(OH)_2$. In $C_{60}(OH)_3$ C1 (not explicitly shown in Fig. 1c) is equivalent to C21 in $C_{60}(OH)_2$ and has as first neighbors C8, C9 and C10, where C9 presents the largest Fermi contact coupling (A_{iso} = 71.63 MHz) while C8 and C10 give A_{iso} = 16.13 MHz, which also satisfy the rule (1) discussed above for $C_{60}OH$. Interestingly, the second neighbors to C1 give negative couplings, obeying the rule (2), the third neighbors are positive, obeying the rule (3), the forth neighbors give negative values, obeying the rule (4), and finally, the fifth neighbors are positive, obeying the rule (5). These rules are sketched in the diagram of Fig. 2b.

As indicated for the C2 site in $C_{60}OH$, the C9 site in $C_{60}(OH)_3$, also belonging to a pentagon ring vertex, is less deshielded ($\delta_{iso} \approx -7$ ppm) than the first neighbors (C8 and C10) in the hexagon ring vertices ($\delta_{iso} \approx -12$ ppm). It is also useful to recall here that the presence of one hydroxyl group at the C1 site ($A_{iso} = -18.15$ MHz) of $C_{60}OH$ produces a coupling constant of 5.27 MHz at C13, whereas in $C_{60}(OH)_3$ the hydroxyl group at the C1 site ($A_{iso} = -20.11$ MHz) practically cancels the coupling constant at C2–OH (see Fig. 2a and c). Also, at C3–OH the hyperfine coupling constant ($A_{iso} = -1.44$ MHz) is relatively negligible. This can be easily related to the spin densities of the doublet states of $C_{60}OH$ and $C_{60}(OH)_3$, displayed in Fig. 3. As is shown, the highest densities are obtained at first neighbors to the OH group, but belonging to pentagon ring vertices. The plots also indicate that the unpaired spins are strongly localized at C2, C5 and C10 in $C_{60}OH$ and, correspondingly, at C9, C32 and C24 in $C_{60}OH_3$. In other words, the presence of the two neighbor OH groups at C1 and C2 does not introduce significant spin densities in their neighborhood.

In summary, we have studied the theoretical ^{13}C NMR properties of low hydroxylated fullerenes in the singlet and doublet states using DFT. From the chemical shifts and Fermi contact couplings, we have pointed out that one single hydroxyl group attached to C_{60} leads to a preferentially localized electron state at the first neighbor carbon site belongs to a pentagon ring vertex of the fullerene cage. Then, adding a second hydroxyl group at this site to form $C_{60}(OH)_2$ we notice a small reduction in the chemical shifts of the vicinal hydroxylated sites in comparison to that of $C_{60}OH$.

Analysis of the chemical shifts in $C_{60}(OH)_2$ reveals that symmetrically opposite sites to the hydroxyl groups are significantly shifted downfield, as well as observed for their first neighbors. This can indicate the high radical reactivity of fullerenols containing few hydroxyl groups and, therefore, a tendency to the polyhydroxylation exhibited by these species. Furthermore, by attaching a third OH group at one of these deshielded opposite sites of $C_{60}(OH)_2$, leading to a $C_{60}(OH)_3$, we have obtained a significant reduction of spin density and, consequently, negligible hyperfine constant couplings at the neighbor hydroxyl groups. This can be interpreted as weak spin couplings in carbon sites containing two vicinal hydroxyl groups. On the contrary, in the neighborhood of the alone hydroxyl group of $C_{60}(OH)_3$ we have obtained a distribution of Fermi contact terms very similar to the case of $C_{60}OH$.

Acknowledgments

This work has been partially supported by the Brazilian agencies CNPq and FAPESP. The authors thank CENAPAD-SP for the computational facilities.

References

[1] M. Bühl, A. Curioni, W. Andreoni, Chem. Phys. Lett. 274 (1997) 231.
[2] P.R. Birkett, M. Bühl, A. Khong, M. Saunders, R. Taylor, J. Chem. Soc. Perkin Trans. 2 (1998) 2037.
[3] T. Sternfeld, F. Wudl, K. Hummelen, A. Weitz, R.C. Haddon, M. Rabinovitz, Chem. Commun. (1999) 2411.
[4] G. Sun, M. Kertesz, J. Phys. Chem. A 104 (2000) 7398.
[5] Z. Chen, W. Thiel, Chem. Phys. Lett. 367 (2003) 15.
[6] G. Sun, Chem. Phys. Lett. 367 (2003) 26.
[7] X. Lu et al., J. Am. Chem. Soc. 130 (2008) 9129.
[8] E. Kleinpeter, S. Klod, A. Koch, J. Org. Chem. 73 (2008) 1498.
[9] J.D. Fortner et al., Environ. Sci. Technol. 41 (2007) 7497.
[10] P.J. Krusic, E. Wasserman, P.N. Keizer, J.R. Morton, K.F. Preston, Science 254 (1991) 1183.
[11] A. Arrais, E. Diana, Fuller. Nanotub. Carbon Nanostruct. 11 (2003) 35.
[12] K. Kokubo, K. Matsubayashi, H. Tategaki, H. Takada, T. Oshima, ACS Nano 2 (2008) 327.
[13] S.T. Yang, H. Wang, L. Guo, Y. Gao, Y. Liu, A. Cao, Nanotechnology 19 (2008) 395101.
[14] T. Helgaker, M. Watson, N.C. Handy, J. Chem. Phys. 113 (2000) 9402.
[15] P. Hrobárik, R. Reviakine, A.V. Arbuznikov, O.L. Malkina, V.G. Malkin, J. Chem. Phys. 126 (2007) 024107.
[16] T.O. Pennanen, J. Vaara, Phys. Rev. Lett. 100 (2008) 133002.
[17] K. Koch, M.C. Holthausen, A Chemists Guide to Density Functional Theory, Wiley VCH, Weinheim, 2001.
[18] K. Wolinski, J.F. Hilton, P. Pulay, J. Am. Chem. Soc. 112 (1990) 8251.
[19] M.J. Frisch et al., Gaussian 98; Revisions A.7 and A.11.4, Inc., Pittsburgh, PA, 1998.
[20] M. Bühl, Chem. Phys. Lett. 267 (1997) 251.
[21] J.A. Pople, W.G. Schneider, H.J. Bernstein, High-resolution Nuclear Magnetic Resonance, McGraw-Hill, New York, 1959.
[22] E.E. Fileti, H.C. Georg, S. Canuto, J. Braz, Chem. Soc. 18 (2007) 74.
[23] O. Walker, P. Mutzenhardt, P. Tekely, D. Canet, J. Am. Chem. Soc. 124 (2002) 865.
[24] J. Czernek, J. Phys. Chem. A 105 (2001) 1357.
[25] R.C. Haddon, Science 261 (1993) 1545.
[26] E.E. Fileti, R. Rivelino, F.B. Mota, T. Malaspina, Nanotechnology 19 (2008) 365703.
[27] Y. Zhang, H. Sun, E. Oldfield, J. Am. Chem. Soc. 127 (2005) 3652.